2003

Material Optimization of Er3+Y2SiO5 at 1.5 μm for Optical Processing, Memory, and Laser Frequency Stabilization Applications

Thomas Böttger
University of San Francisco, tbottger@usfca.edu

Y Sun

C W. Thiel

R L. Cone

Recommended Citation
Thomas Böttger ; Yongchen Sun ; Charles W. Thiel and Rufus L. Cone. "Material optimization of Er3+:Y2SiO5 at 1.5 μm for optical processing, memory, and laser frequency stabilization applications", Proc. SPIE 4988, Advanced Optical Data Storage, 51 (June 30, 2003); doi:10.1117/12.474784

Material Optimization of $Er^{3+}:Y_2SiO_5$ at 1.5 μm for Optical Processing, Memory, and Laser Frequency Stabilization Applications

Thomas Böttger, Y. Sun, C. W. Thiel, and R. L. Cone
Physics Department, Montana State University, EPS 264, Bozeman, MT 59717

ABSTRACT

Spatial-spectral holography using spectral hole burning materials is a powerful technique for performing real-time, wide-bandwidth information storage and signal processing. For operation in the important 1.5 μm communication band, the material $Er^{3+}:Y_2SiO_5$ enables applications such as laser frequency stabilization, all-optical correlators, analog signal processing, and data storage. Site-selective absorption and emission spectroscopy identified spectral hole burning transitions and excited state T_1 lifetimes in the 1.5 μm spectral region. The effects of crystal temperature, Er^{3+}-dopant concentration, magnetic field strength, and crystal orientation on spectral diffusion were explored using stimulated photon echo spectroscopy, which is the "prototype" interaction mechanism for device applications. The performance of $Er^{3+}:Y_2SiO_5$ and related Er^{3+} materials has been dramatically enhanced by reducing the effect of spectral diffusion on the coherence lifetime T_2 through fundamental material design coupled with the application of an external magnetic field oriented along specific directions. A preferred magnetic field orientation that maximized T_2 by minimizing the effects of spectral diffusion was determined using the results of angle-dependent Zeeman spectroscopy. The observed linewidth broadening due to spectral diffusion was successfully modeled by considering the effect of one-phonon (direct) processes on Er^{3+} - Er^{3+} interactions. The reported studies improved our understanding of Er^{3+} materials, explored the range of conditions and material parameters required to optimize performance for specific applications, and enabled measurement of the *narrowest* optical resonance ever observed in a solid—with a homogeneous linewidth of 73 Hz. With the optimized materials and operating conditions, photon echoes were observed up to temperatures of 5 K, enabling 0.5 GHz bandwidth optical signal processing at 4.2 K and providing the possibility for operation with a closed-cycle cryocooler.

Keywords: optical coherent transients, spectral hole burning, spectral diffusion, signal processing, Erbium, 1.5 μm wavelength

1. INTRODUCTION

Many computing and communication systems require real-time, wide-bandwidth information storage and signal processing solutions that can be achieved using spatial-spectral holography in rare-earth-activated materials. In addition to possessing all the capabilities of traditional spatial holography, spatial-spectral holography exploits frequency selectivity to record and process the spectral and temporal characteristics of the incident light field, extending the concepts of holography to the additional dimension of frequency or time. Spectral hole burning (SHB) in rare-earth materials provides the intrinsic frequency selectivity required by practical information processing applications.[1] For example, these materials can coherently process phase and amplitude modulated analog signals at GHz to THz rates with time delays up to milliseconds. Rare-earth materials also enable data storage applications with demonstrated density-bandwidth products in excess of 100,000 terabits per square inch per second with microsecond latency.[2] Recently, it has been established that rare-earth materials offer outstanding frequency references for laser stabilization needed in both fundamental spectroscopy and device applications, with demonstrated stabilities of 1 part in 10^{13} of the optical frequency over 10 ms timescales.[3] These same rare-earth-activated materials are also promising candidates for quantum information applications.[4]

Spatial-spectral holographic materials are inhomogeneously broadened absorbers; the absorption line of the bulk material consists of an ensemble of much narrower absorption lines corresponding to subgroups of ions in the crystal. Small variations in the crystalline environment of each ion create a static distribution of resonant frequencies that gives rise to the inhomogeneously broadened absorption line. The fundamental absorption linewidth of each subgroup that contributes to the inhomogeneous line is called the homogeneous linewidth and can be as narrow as 73 Hz at optical

frequencies, as reported here. Devices incorporating these materials may be programmed with light to perform a variety of functions over the spectral region of the inhomogeneous absorption linewidth, which can span from sub-GHz to several hundreds of GHz in crystalline solids or up to several THz in glasses. When a narrow spectral region of the bulk absorption is saturated by a laser, notches or spectral holes are "burned" into the line shape, modifying the optical properties of the medium. Spectral hole burning can be used in the time domain to store temporally structured optical pulse patterns as a spectral modulation of the population in the ground and excited state of the inhomogeneously broadened medium. Stored data pulse patterns can be recalled using stimulated photon echoes, leading to optical memory with a storage duration at low temperatures ranging from microseconds in some materials to weeks or longer in others. Using the stimulated photon echo approach, the re-programming or refresh time of a recorded data stream is established by the material's optical coherence lifetime T_2 and population lifetime T_1. Even with continuous programming and accumulation,[5,9] T_2 remains one of the most important parameters for SHB applications. In addition to improving our fundamental understanding of these materials, detailed studies of the crystal properties that influence the coherence lifetime also directly advance the development of performance-optimized materials for device applications.

2. Er^{3+}:Y_2SiO_5

The material Er^{3+}:Y_2SiO_5 plays an important role in rare-earth-based SHB devices covering the telecommunication band at 1.5 μm. In this material, SHB at 1.5 μm occurs for the lowest $^4I_{15/2} \rightarrow {}^4I_{13/2}$ transition by population storage in the long-lived $^4I_{13/2}$ excited state. In 1997, the first two-pulse photon echoes with observed coherence lifetimes up to 580 μs were measured in our laboratory,[6] triggering a number of SHB proof-of-principle device demonstrations, including real-time address header decoding for optical data routing,[7] spatial-spectral holographic correlation,[8] as well as applications in laser frequency stabilization.[3] Recently, the material optimization reported in this paper allowed the demonstration of much higher bandwidth (0.5 GHz) analog signal processing at temperatures of 4.2 K.[9] These demonstrations were motivated by the desire to develop SHB technologies that enable all-optical memory, switching, and processing at communication wavelengths[1] and exploit telecom hardware for more general SHB-based applications. The material Er^{3+}:Y_2SiO_5 has also been investigated for solid-state laser applications[10] due to its good chemical and thermo-mechanical properties as well as its potential for high rare-earth doping. Our experimental and theoretical work has significant impact on these applications as well.

The crystal Y_2SiO_5 (also called yttrium silicate or YSO) belongs to the space group C_{2h}^6 (C2/c, number 15) with eight formula units per monoclinic cell. The Y^{3+} ions occupy two crystallographically inequivalent sites of C_1 symmetry[11] and the Er^{3+} ions substitute for Y^{3+} host ions at both crystallographic sites without charge compensation. All crystals were grown by Scientific Materials Corp. (Bozeman, MT) using the Czochralski method and were transparent and colorless. There are 3 mutually perpendicular optical extinction axes in Y_2SiO_5; the ***b***-axis is parallel to the ⟨010⟩ direction and the $\boldsymbol{D_1}$ and $\boldsymbol{D_2}$ axes correspond to the optical extinction directions when the crystal is viewed along ⟨010⟩ between crossed polarizers.[10] All crystals were x-ray oriented, cut perpendicular to the three optical extinction axes, and polished to optical quality.

3. SITE-SELECTIVE SPECTROSCOPY

An earlier study of Er^{3+}:Y_2SiO_5 within the context of solid-state laser material development was reported by Li *et. al*;[10] however, the spectroscopic measurements reported there did not differentiate between crystallographic sites. In the present study, site-selective spectroscopy experiments with continuously tunable external cavity diode lasers (ECDL) were used to identify the $^4I_{15/2}$ ground state and $^4I_{13/2}$ excited state crystal field levels for both Er^{3+} sites and to identify relevant spectral hole burning transitions at 1.5 μm. Absorption measurements located the excited-state crystal field levels, and site-selective fluorescence unambiguously assigned the excited and ground state level structure to Er^{3+} ions occupying either crystallographically inequivalent Y^{3+} site.

For absorption, a 2 % Er^{3+}:Y_2SiO_5 crystal was held at low temperature (2 K) to ensure that only the lowest crystal field level Z_1 of the $^4I_{15/2}$ ground J-multiplet was significantly populated. The crystal was aligned with its ***b***-axis parallel to the light propagation direction, a Glan-Thompson polarizer was used to select the light polarization, and light transmitted through the crystal was analyzed with a 1.0 m spectrometer and detected with a cooled germanium detector.

Atmospheric water vapor lines were used to precisely calibrate the wavelength of the absorption spectrum.[12] Calibration for other measurements was verified using a narrowband external cavity diode laser (ECDL) as a marker whose wavelength was determined with an accuracy of ± 100 MHz using a Burleigh WA 1500 wavemeter.

Absorption lines to the crystal field levels of the $^4I_{13/2}$ J-multiplet are shown in Fig. 1. The sharp well-resolved lines determined 13 of the 14 levels in the $^4I_{13/2}$ J-multiplets for the two sites. The absorption lines from the two Er^{3+} sites are interspersed, with each site experiencing different crystal field splittings.

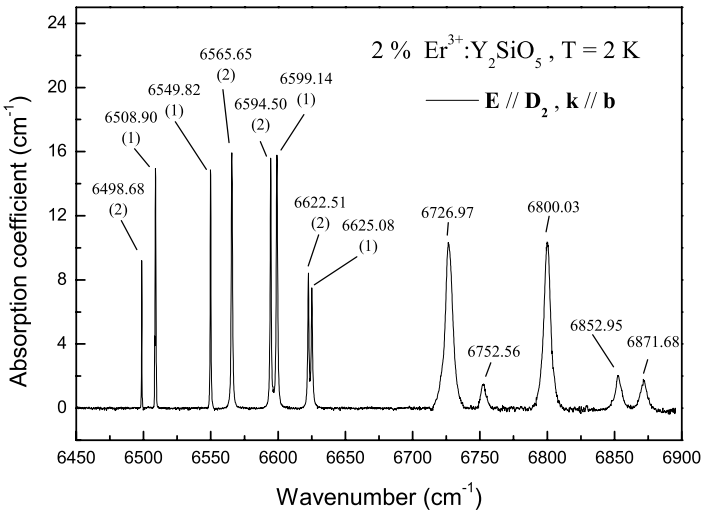

Figure 1: Polarized absorption spectrum of 2% Er^{3+}:Y_2SiO_5 for E//D_2 at T = 2 K. Line centers and crystallographic site assignments (in parenthesis) are given.

Two distinct fluorescence spectra, each corresponding to a specific crystallographic site, were observed when pumping each absorption line with the narrowband ECDL, allowing the crystal field levels of the $^4I_{15/2}$ and $^4I_{13/2}$ multiplets to be assigned to site 1 or site 2; line centers and site assignments are indicated in the figure. The limited tuning range of the ECDL used in these experiments prevented pumping levels above $^4I_{13/2}$:Y_4 so that levels above 6700 cm^{-1} could not be assigned. A complete report and discussion of these measurements will be presented elsewhere.[13,14]

4. LIFETIME MEASUREMENTS

Knowledge of the excited state lifetime T_1 is important since it establishes the ultimate limit for the coherence lifetime T_2 through the relation $T_2 \leq 2T_1$ and establishes the spectral hole lifetime for population storage in the excited state. The fluorescence dynamics of the metastable $^4I_{13/2}$:Y_1 excited state were investigated for Er^{3+} in both crystallographic sites. Figure 2 shows the measured $^4I_{13/2}$:$Y_1 \rightarrow {}^4I_{15/2}$:$Z_1$ fluorescence decay for site 1 at a temperature of 10 K. The decays were exponential over three decades and exponential least-squares fits gave fluorescence lifetimes $T_1 = 11.4$ ms for site 1 and $T_1 = 9.2$ ms for site 2. The ultra-low Er^{3+} concentration of 0.001 % used in our experiments minimized the effect of radiation trapping on the observed fluorescence lifetimes. The nearly negligible effect of radiation trapping was confirmed by the minimal effect of temperature and excitation energy on the observed lifetimes; hence, these measured values establish an upper limit for the fluorescence lifetime of the $^4I_{15/2}$:Y_1 level in Er^{3+}:Y_2SiO_5 materials.

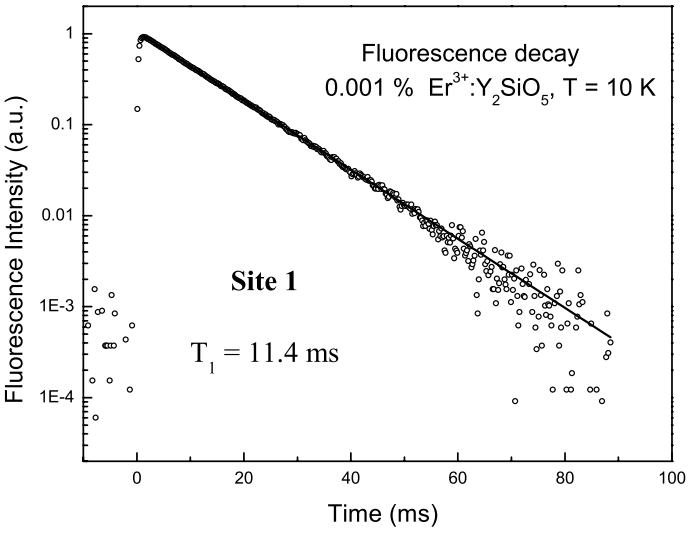

Figure 2: Fluorescence decay of site 1 for the 0.001 % Er^{3+}:Y_2SiO_5 $^4I_{13/2}(Y_1) \rightarrow {}^4I_{15/2}(Z_1)$ transition at T = 10 K.

5. OPTICAL DEPHASING AND ZEEMAN EXPERIMENTS

Optical interactions with rare-earth-activated materials rely on the macroscopic polarization created by the combined response of the individual rare-earth ions in the material. The macroscopic polarization and resulting material response depend on the phase relationships between the individual ions. To enhance processing time or storage density, the coherence time should be maximized under practical operating conditions. For Er^{3+} optical centers, loss of phase coherence between the ions is induced by random perturbations of the energy levels involved in the optical transition, a process that also contributes to spectral diffusion. In Er^{3+}:Y_2SiO_5, the primary source for dephasing is the magnetic dipole-dipole interaction between the large magnetic moments of the Er^{3+} ions' electronic states. The energy of each Er^{3+} ion depends on the orientation of all other Er^{3+} moments in the crystal; therefore, whenever an Er^{3+} ion undergoes a spin flip, it perturbs the energy levels of the other ions in its environment. To achieve long coherence lifetimes, it is necessary to suppress the spin flips of all Er^{3+} ions in the crystal, including both the optically active Er^{3+} ions that are directly probed by the laser as well as all remaining non-resonant Er^{3+} ions in the environment. The application of an external magnetic field lifts the Kramers degeneracy, "freezing out" spin flips through the preferential occupation of the lower energy spin state. The ratio of the level splitting to the available thermal energy $g\mu_B B/kT$ is a key variable influencing the microscopic dynamics in Er^{3+}:Y_2SiO_5. Maximizing the level splitting at a particular applied field requires knowledge of the anisotropy of the ground and excited state Er^{3+} magnetic moments at each site. As a fundamental part of the material optimization strategy, this magnetic anisotropy was measured using Zeeman spectroscopy as a function of magnetic field orientation to determine the relevant ground and excited state g-values.

Simultaneously maximizing the g-values for the ground and excited states of all ions that influence the optical dephasing was challenging due to the complex crystal structure of Er^{3+}:Y_2SiO_5, which has two distinct crystallographic sites, each exhibiting the lowest C_1 site symmetry. Additional complexity arises from the magnetic inequivalence of the multiple orientations that occur for each of the crystallographic sites within the unit cell. The results of Zeeman spectroscopy identified a preferred magnetic field orientation at an angle of $\Phi \sim 140^o$ with respect to the $\boldsymbol{D_1}$-axis in the $\boldsymbol{D_1}$-$\boldsymbol{D_2}$ plane.[15] This direction minimizes the spin flips of ions at both site 1 and site 2. A full report of these measurements will be given elsewhere.[13,14]

Two-pulse photon echo experiments were performed as a function of magnetic field orientation to measure the optical dephasing and to confirm the elaborate predictions derived from the Zeeman experiments. Optical dephasing for site 1 in a 0.001 % Er^{3+}:Y_2SiO_5 crystal was measured as a function of magnetic field orientation in the $\boldsymbol{D_1}$-$\boldsymbol{D_2}$ plane at 1.6 K with a magnetic field of 3 T. The experimental apparatus and conditions were the same as for stimulated photon echo spectroscopy described below. Under these experimental conditions, linewidth values spanned over two orders of magnitude from 400 Hz to 50 kHz as the magnetic field orientation was varied, highlighting the leading role of Er^{3+} spin flips as a source of optical dephasing. As predicted by our optimization strategy, the narrowest homogeneous linewidths of ~ 400 Hz were observed for magnetic field orientations of $\Phi \sim 140^o - 160^o$ with respect to the $\boldsymbol{D_1}$-axis in the $\boldsymbol{D_1}$-$\boldsymbol{D_2}$ plane. This confirms that the spectral diffusion may be suppressed using knowledge of the magnetic anisotropy to select orientations that simultaneously maximize the level splittings of both site 1 and site 2. The two-pulse echo results demonstrated further that non-resonant "environment" ions at both crystallographic sites contribute to dephasing and must be considered in the selection of the preferred external magnetic field orientation. An additional criterion for choosing the magnetic field direction is to maximize the number of magnetically equivalent Er^{3+} ions to enhance the interaction with the resonant optical field.[15] For Er^{3+}:Y_2SiO_5, applying the magnetic field in the $\boldsymbol{D_1}$-$\boldsymbol{D_2}$ plane, which contains the preferred direction discussed above, increases the number of ions resonant with the laser by a factor of two compared to an arbitrary field orientation. A full discussion of these measurements will be presented elsewhere.[13,14]

6. STIMULATED PHOTON ECHO SPECTROSCOPY AND SPECTRAL DIFFUSION

Intrinsic frequency selectivity of SHB materials enables the storage and manipulation of information encoded in the spectral or temporal properties of the light field. To analyze the material response over timescales appropriate for SHB applications, we extensively characterized the evolution of the coherence lifetime and spectral hole linewidth, both of which vary with time due to the presence of spectral diffusion in Er^{3+}:Y_2SiO_5. The angle-dependent Zeeman spectroscopy and two-pulse photon echo decay experiments identified preferred directions for the magnetic field that minimized dephasing induced from neighboring ions of site 1 and site 2. Additional information on the Er^{3+} dynamics

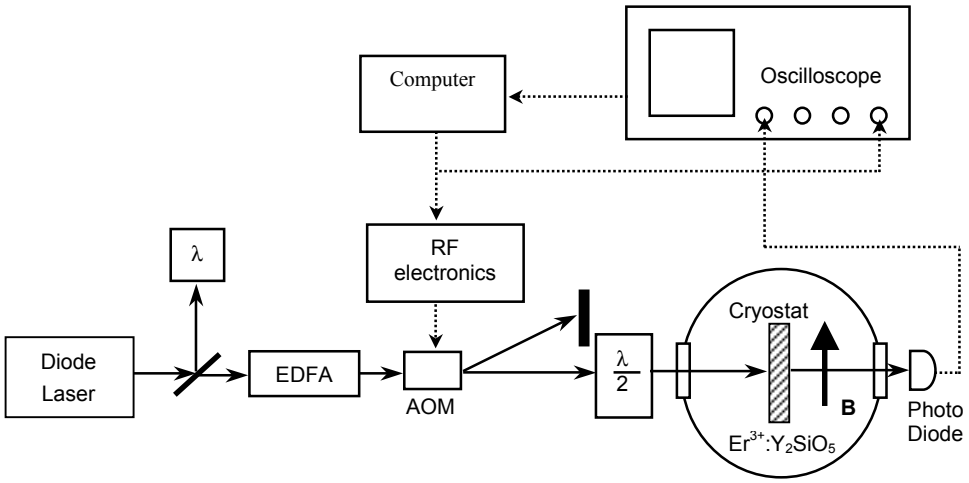

Figure 3: Experimental setup for measuring two-pulse photon echoes and stimulated echoes.

was extracted by studying the dephasing of the optical center with stimulated photon echo spectroscopy. This method was ideal for investigating the effect of spectral diffusion on the linewidth over the timescales of interest for practical SHB device applications. These measurements also guided the choice of Er^{3+} concentration, magnetic field strength, and operating temperature for optimizing the material and provided insight into the microscopic spin dynamics.

The Er^{3+}:Y_2SiO_5 crystals were aligned with the light propagating along the ***b***-axis and with the magnetic field along $\boldsymbol{D_1}$. The experimental apparatus is depicted in Fig. 3. The laser (ECDL) output power of ~ 1.8 mW was amplified by an Erbium doped fiber amplifier to 35 mW. An acousto-optic modulator (AOM) gated the photon echo pulse-sequence from the amplified laser beam. For most experiments, the beam was focused inside the crystal to a waist of radius ~ 25 μm. Typical π/2-pulse widths were ~ 500 ns, giving a ~ 2 MHz spectral width that minimized the sensitivity of the measurements to laser frequency fluctuations. The observed photon echo signals were detected using a photodiode.

The stimulated photon echo employs a three-pulse sequence and can be thought of as a modified two-pulse echo with a pulse delay of t_{12}, where the second π-pulse is broken up into two π/2-pulses that are separated by the waiting time T_W. Figure 4 shows an actual stimulated photon echo pulse sequence. As in the two-pulse echo case, the first pulse prepares the ions by placing each ion in a coherent superposition of the ground and excited state. During the delay t_{12}, the phase of the superposition state evolves according to the ion's instantaneous transition frequency. The second pulse stores each ion's total accumulated phase as a population difference between the ground and excited states. Thus, a frequency dependent population grating is produced between the ground and excited states with a period given by $1/t_{12}$. This grating decays due to population decay with the lifetime of the excited state T_1. In addition, spin-flips of other Er^{3+} ions in the crystal cause

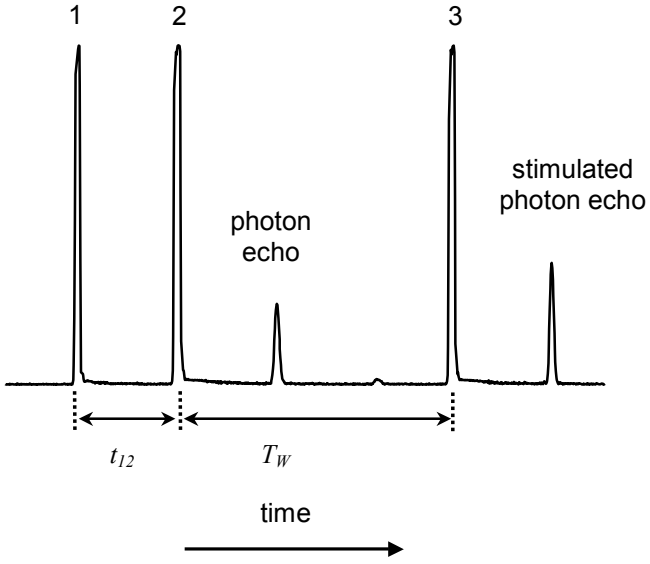

Figure 4: A typical stimulated photon echo pulse sequence. The first two excitation pulses are separated by a time delay t_{12} and pulse 2 and 3 are separated by the waiting time T_W. The stimulated photon echo occurs at a time delay t_{12} after pulse 3, a two-pulse echo can be observed at a time delay t_{12} after pulse 2; note that the excitation pulse area is ~ π/2 for each of the three pulses, causing the stimulated photon echo to be stronger than the two-pulse photon echo.

frequency shifts in the levels of the individual ions that make up the population grating. These frequency shifts tend to smear out the grating (i.e. spectral diffusion) and therefore lead to a loss of the stored coherence. When a short π/2-pulse is applied after the waiting time T_W, the remaining coherence stored in the population grating is rephased after an additional time delay of t_{12} and a stimulated photon echo is emitted. The stimulated photon echo intensity contains information about dephasing during the two t_{12} delays and spectral diffusion and population decay during T_W. Systematic measurements of the stimulated echo intensity I were made as t_{12} was varied for different T_W to map out the time evolution of the effective homogeneous linewidth Γ_{eff} as excited ions underwent spectral diffusion.

A specific spectral diffusion model has been incorporated into the echo decay function, enabling us to significantly extend previous data analysis methods.[16] In this model, a generalized form of the echo decay function

$$I(t_{12},T_W) = A\cdot\exp\left\{-\frac{2T_W}{T_1}\right\}\cdot\exp\left\{-4t_{12}\pi\,\Gamma_{eff}(t_{12},T_W)\right\} \tag{1}$$

describes the stimulated echo intensity, where the constant homogeneous linewidth is replaced by a time-dependent effective linewidth $\Gamma_{eff}(t_{12},T_W)$ that incorporates the effect of spectral diffusion. If we specifically consider the spectral diffusion resulting from spin flips, the effective linewidth is given by

$$\Gamma_{eff}(t_{12},T_W) = \Gamma_0 + \tfrac{1}{2}\Gamma_1\left[R\,t_{12} + \left\{1-\exp\left(-RT_W\right)\right\}\right], \tag{2}$$

following the approach of Mims.[17] In this expression, Γ_0 is the initial homogeneous linewidth in the absence of spectral diffusion, Γ_1 is the maximum contribution of spectral diffusion to the homogeneous linewidth, and R is the rate of perturbations causing the spectral diffusion. This expression is valid in the limit $Rt_{12} \ll 1$; for the limit $Rt_{12} \gg 1$, the effective linewidth is expected to be independent of T_W. Analyzing the behavior of the physical parameters R and Γ_1 extracted from the data using this approach provides direct insight into the microscopic dynamics causing the spin flips and also allows the effect of spectral diffusion to be predicted and explained for a wide range of operating conditions. The underlying theory as well as experimental detail will be presented elsewhere.[13,18]

If we analyze the spectral diffusion that occurs during T_W, Eq. (2) simplifies to

$$\Gamma_{eff}(T_W) = \Gamma_0 + \tfrac{1}{2}\Gamma_1\left[1-\exp\left\{-RT_W\right\}\right], \tag{3}$$

allowing the effective homogeneous linewidth to be modeled as a function of T_W from the stimulated echo decay curves. This expression represents the effective initial linewidth for very short t_{12} and also approximately describes the behavior of the effective linewidth for cases where the linewidth is dominated by spectral diffusion during the waiting time, as is the case for large T_W. In the long time limit, Eq. (1) and Eq. (3) predict simple exponential decays with a saturated effective linewidth given by $\Gamma_0 + \frac{1}{2}\Gamma_1$, where the factor of $\frac{1}{2}$ enters because spectral diffusion during the waiting time only produces dephasing for the last t_{12} section of the echo sequence. It is important to note that the corresponding absorption linewidth is a Lorentzian with a full width at half maximum given by $\Gamma_0 + \Gamma_1$.

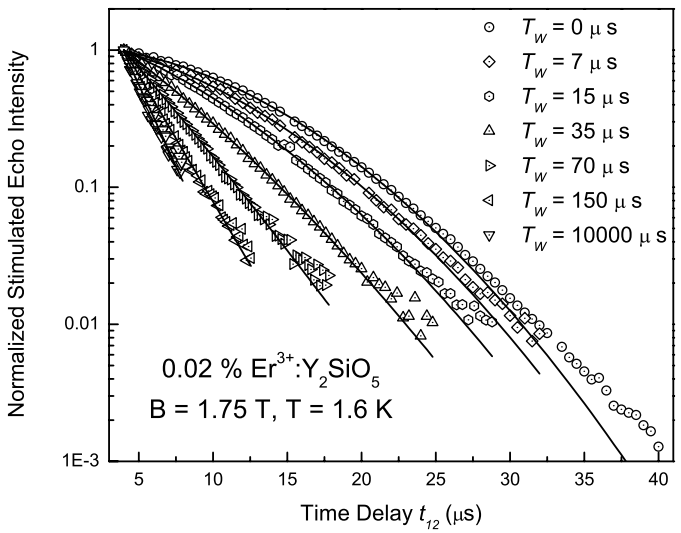

Figure 5: Stimulated photon echo decays for 0.02% Er^{3+}:Y_2SiO_5 in a magnetic field of B = 1.75 T at 1.6 K as the waiting time is varied between 0 μs and 10000 μs; $\boldsymbol{B}$ // $\boldsymbol{D_1}$. Solid lines are least-square fits to Eq. (1), with Γ_{eff} given by Eq. (2).

Figure 5 shows typical stimulated photon echo decays for 0.02 % Er^{3+}:Y_2SiO_5 in a magnetic field of 1.75 T and at 1.6 K as T_W was varied from 0 μs (equivalent to a two-pulse photon echo decay) to 5000 μs. Stimulated photon echo decays for short waiting times were non-exponential, indicating the rapidly increasing effect of spectral diffusion occurring on the time scale of the echo sequence.

Longer waiting times yielded exponential decays, and the observed decay constants saturated at values determined by the temperature, concentration, magnetic field, and field direction. The solid lines are fits to the data points using Eq. (1) with Γ_{eff} given by Eq. (2); they gave good agreement, allowing the time evolution of the linewidth to be extracted as the waiting time T_W was varied. It should be noted that this model tends to underestimate the echo intensity at large values of t_{12}, as can be seen by a small deviation of the fit from the data for the first three curves (T_W = 0 μs, 7 μs, 15 μs). For these decay curves, the value of t_{12} approaches $1/R$, corresponding to a significant probability for each perturber to undergo multiple spin flips during the t_{12} sections of the echo sequence. Perturbers that undergo multiple spin flips have a reduced effect on the optical dephasing since the dephasing induced by subsequent flips tends to cancel, reducing the net effect. This causes the echo intensity to decay more slowly as t_{12} approaches $1/R$, an effect similar to "motional narrowing" in NMR.

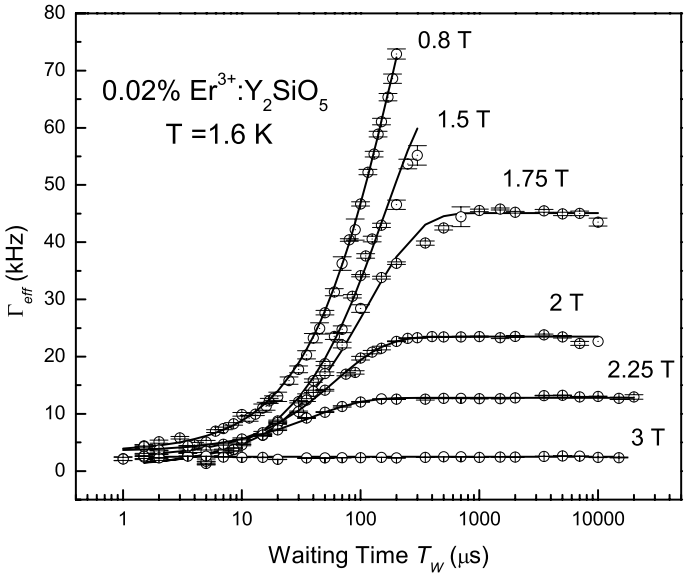

Figure 6: Evolution of the effective linewidth of site 1 in 0.02 % Er^{3+}:Y_2SiO_5 at 1.6 K as the waiting time T_W is varied in a stimulated photon echo experiment. The magnetic field varies from B = 0.8 T to B = 3 T between data sets; $\boldsymbol{B} \,//\, \boldsymbol{D_1}$. Solid lines are least-squares fits to the data using Eq. (3).

Representative results of the stimulated echo analysis are shown in Fig. 6 for a 0.02 % Er^{3+}:Y_2SiO_5 sample, where the evolution of the effective linewidth is mapped as a function of T_W for a variety of magnetic fields from 0.8 T up to 3 T at 1.6 K. Solid lines in the figure are least-squares fits to the data using Eq. (3). Each case shows excellent agreement. The presence of spectral diffusion is clearly observed in the significant broadening of the linewidth as T_W is increased. For these measurements, a plateau was reached after several hundred microseconds where the contribution of spectral diffusion to the linewidth reached its saturated value. As shown in Fig. 6, a larger magnetic field dramatically suppresses linewidth broadening, illustrating how the magnetic field strength may be chosen to reduce the linewidth to a particular level required for a given application.

To understand and predict the behavior of the spectral diffusion as a function of magnetic field and temperature, we employed a specific model based on the spin-flip dynamics in the material. The spectral diffusion parameters Γ_1 and R may be modeled by considering the magnitude of the dipole-dipole interactions between Er^{3+} ions and the physical mechanism driving the spin flips. The model predicts saturation of the linewidth when all spins deviating from thermal equilibrium have flipped. The saturated linewidth value $\Gamma_1(B,T)$ for long T_W is related to the size of the average deviation of the population from equilibrium and is given by

$$\Gamma_1(B,T) = \Gamma_{\max} \operatorname{sech}^2\left(\frac{g\mu_B B}{2kT}\right), \tag{4}$$

where g is the g-value of the ground state Kramers doublet, μ_B the Bohr magneton, B the magnetic field, k the Boltzmann constant, T the temperature, and $\Gamma_{\max}$ is determined by the magnitude of the dipole-dipole interaction between Er^{3+} ions. It is important to note that, for magnetic dipole-dipole interactions between ions randomly distributed in the crystal lattice, $\Gamma_{\max}$ may be calculated from knowledge of the crystal structure and the magnitude of the dipole moments in the ground and excited states.[17,19] The ratio $\Delta E_g / 2kT = g\mu_B B / 2kT$ between the ground state energy level splitting ΔE_g and the thermal energy available to the ions kT determines the saturation level of the homogeneous linewidth Γ_1. If the splitting is large compared to the thermal energy, deviations of the spin population from thermal equilibrium will be small and therefore only make a negligible contribution to the spectral diffusion of the optical center.

The spectral diffusion rate R represents the sum of the upward and downward spin-flip transition rates and is given by the spin-lattice relaxation rate that describes how fast the spin population returns to thermal equilibrium. To model the behavior of R, we must explicitly incorporate the mechanism driving the spin flips. If we attribute the driving mechanism to the one-phonon (direct) absorption and emission process between the two Zeeman levels, the relaxation rate for Kramers ions as a function of magnetic field and temperature is given by[20]

$$R(B,T) = R_0 + \alpha (g\mu_B)^3 B^5 \coth\left(\frac{g\mu_B B}{kT}\right), \qquad (5)$$

where α is a constant determined by the phonon coupling, R_0 is the spin-flip rate at zero magnetic field, and all remaining quantities are the same as in Eq. (4). Physically, R_0 corresponds to the minimum spin-lattice relaxation rate, and it results from mechanisms that have negligible dependence on the applied magnetic field strength over the range studied, such as two-phonon interactions with higher energy electronic states. Over the temperature and magnetic field ranges studied here, R_0 typically represents a small contribution to the observed rates. The spin-lattice relaxation rate described by Eq. (5) grows rapidly with increasing magnetic field strength due to an increase of the accessible density of phonon states at energies degenerate with the splitting of the Zeeman levels and an increase in the magnetic-field-induced wavefunction mixing of crystal field levels.

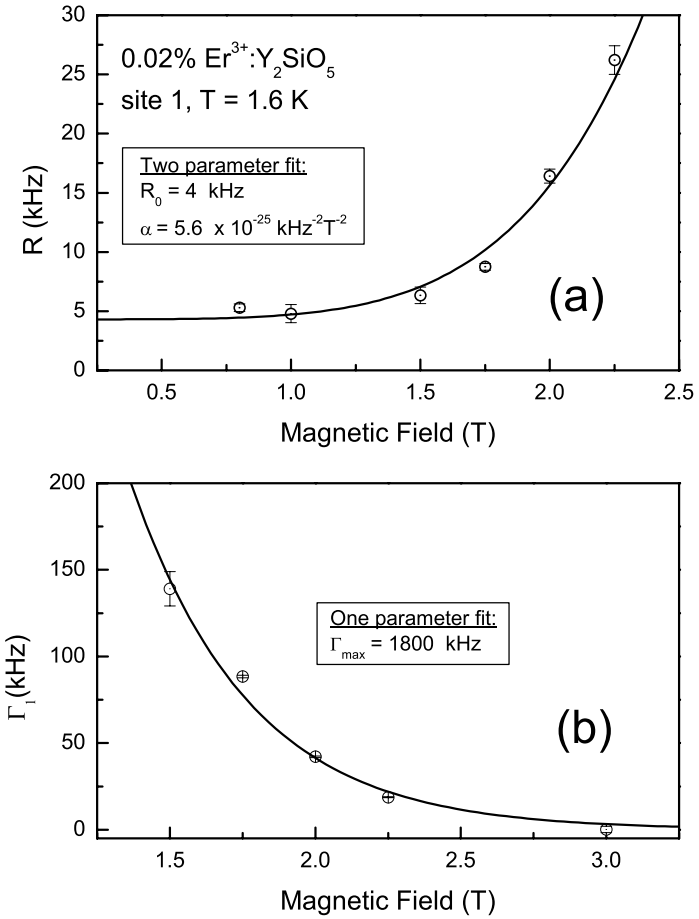

Figure 7: (a) Measured relaxation rate R and (b) saturated spectral diffusion linewidth Γ_1 as a function of magnetic field for 0.02% Er^{3+}:Y_2SiO_5 at 1.6 K; $\boldsymbol{B} // \boldsymbol{D_1}$. Solid lines are least-squares fits using equations Eq. (5) and Eq. (4), respectively.

Field dependent linewidth saturation values $\Gamma_1(B)$ and relaxation rates $R(B)$ obtained from the fits shown in Fig. 5 are plotted with error bars as a function of magnetic field in Fig. 7. The solid lines are least-squares fits to the magnetic field dependent saturated linewidth $\Gamma_1(B)$ and rate $R(B)$ using Eq. (4) and Eq. (5), respectively. Both fits give excellent agreement and fitting parameters are shown in the figure. For these fits, the exact measured g-value of g = 6.1 for site 1 with $\boldsymbol{B} // \boldsymbol{D_1}$ was used, clearly indicating that the spectral diffusion was dominated by spin flips of environment ions occupying site 1. Spin flips of site 2 were "frozen out" due to the much larger ground state energy level splitting for this $\boldsymbol{B} // \boldsymbol{D_1}$ direction (g = 14.7). We also observed that spectral diffusion of site 1 can be dominated by spin flips from either site 1 or site 2 for different magnetic field orientations, consistent with the measured magnetic anisotropy.

Spectral diffusion was also investigated at elevated temperatures. In a 0.005% Er^{3+}:Y_2SiO_5 crystal held at T = 4.2 K in a field of B =3 T, spectral diffusion was evident as Γ_{eff} broadened from ~ 20 kHz to ~ 110 kHz within the first 20 μs and then saturated. Stimulated echoes were consistently measurable over the entire lifetime of the excited state for waiting times up to T_W = 10 ms. These optimized material properties, coupled with a laser stabilized to a spectral hole frequency reference,[3] enabled high bandwidth (0.5 GHz) signal processing in that crystal at 4.2 K, providing the possibility for operation with a closed-cycle cryocooler.[9]

The success of this analysis allows us to not only identify the source of spectral diffusion as Er^{3+} ions residing at site 1, but also allows us to identify the specific mechanism responsible for the spectral diffusion as spin flips driven by the

one-phonon process. It should be noted that spectral diffusion due to Y^{3+} ion nuclear spin flips, with rates on the order of a few Hz,[21] occurs on a timescale longer than our stimulated photon echo measurements, but is expected to contribute significantly to the linewidth broadening on timescales of hundreds of milliseconds or longer. By extending this analysis to related materials, new insight into the physical mechanisms that influence each material's behavior may be gained.

A detailed description of the elaborate experimental results on spectral diffusion that include systematic measurements with Er^{3+} ion concentration, magnetic field, and temperature, will be reported elsewhere.[13,18]

7. ULTRASLOW DEPHASING

Guided by our material optimization strategy that suppresses optical dephasing, we investigated the material coherence time (or homogeneous linewidth) under optimum experimental operating conditions in the crystal with 0.001 atomic percent Er^{3+} concentration. Dephasing for site 1 was characterized using two-pulse photon echo measurements with a magnetic field of 7 T applied in the $\boldsymbol{D_1}$-$\boldsymbol{D_2}$ plane and with the laser propagation direction along the $\boldsymbol{b}$-axis. The magnetic field was oriented along the preferred direction of $\boldsymbol{\Phi} = 140^{o}$ with respect to the $\boldsymbol{D_1}$ crystal axis. To "freeze out" the thermal population in the upper Zeeman level of the ground state, the sample was immersed in a liquid helium bath held at 1.5 K. Under these conditions, two-pulse echo decays gave a dephasing time of $T_2 = 4.38$ ms, corresponding to an optical homogeneous linewidth of 73 Hz.[13,18] This is the longest optical dephasing time ever measured in any solid-state material, with the corresponding linewidth being the narrowest optical resonance. Residual contributions to this narrow linewidth are population decay, excitation induced dephasing (instantaneous spectral diffusion),[19] and contributions from the ^{89}Y nuclear spin fluctuations. The excited state lifetime $T_1 = 11.4$ ms establishes the ultimate limit of 14 Hz for the homogeneous linewidth in Er^{3+}:Y_2SiO_5. Further measurements are required to separate other individual contributions, which may include fluctuations in laser frequency stability, fluctuations of the earth's magnetic field, or stray electromagnetic fields in the laboratory as suggested by the results of Equall *et. al.*[22], where a linewidth of $\Gamma_{hom} = 122$ Hz was measured in Eu^{3+}:Y_2SiO_5.

8. SUMMARY AND CONCLUSION

Optical material design and the choice of practical operating conditions require a complex balance of many factors that must be simultaneously satisfied for each specific application. Developing a buffer memory, for example, might require high spectral bandwidth and strong optical transition dipoles for high Rabi frequencies, while ultra-dense data storage might require longer coherence and spectral hole lifetimes. Applications requiring maximum signal sensitivity and compactness may benefit from higher dopant concentrations to increase the interaction strength; however, the higher concentrations also increase the spectral diffusion, resulting in broader homogeneous linewidths and shorter coherence lifetimes. Every device implementation must be analyzed to determine an optimal balance between design parameters as diverse as optical wavelength, absorption strength, Rabi frequency, coherence lifetime, inhomogeneous linewidth, hole burning efficiency, spectral hole lifetime, laser power, operating temperature, and magnetic field strength.

The work reported here explores aspects of rare-earth-activated materials that are critical for SHB-enabled optical technologies. These experimental studies provide the basis for theoretical understanding of how the material properties are affected by the operating conditions. Both the advanced modeling and the determination of the static and dynamic optical properties have been illustrated here. By fully understanding the behavior of spectral diffusion and its effect on material performance, precise operating conditions and material composition can be chosen to meet specific requirements for each device application.

An extensive study of the material Er^{3+}:Y_2SiO_5 has been carried out to improve our fundamental understanding of the dynamic interactions responsible for spectral diffusion and to use this information to obtain longer coherence lifetimes crucial for SHB device applications. Based on the experimental evidence and our understanding of the material physics, an optimization strategy was developed that is also applicable to similar Er^{3+} materials and other paramagnetic ions. To minimize dephasing, the g-values must be simultaneously maximized in both the ground and excited states for all crystallographic sites in the material. In addition, the site exhibiting the longest T_1 lifetime and strongest absorption should be used for SHB applications. Magnetic field strength and operating temperature can then be employed to

"freeze out" the thermal spin population in upper Zeeman levels. The magnetic field should also be oriented so that a minimum of magnetically inequivalent site orientations is present in the crystal. The Er^{3+} concentration can be adjusted to increase Er^{3+} - Er^{3+} ion distances and reduce spectral diffusion while balancing the necessity for sufficient optical absorption.

Our study led to significant material optimization that allowed demonstration of high bandwidth (0.5 GHz) optical signal processing[9] at T = 4.2 K and also enabled the measurement of what we believe to be the narrowest optical resonance in a solid with a homogeneous linewidth of 73 Hz.

ACKNOWLEDGEMENTS

The authors are grateful to Randy W. Equall and Ralph L. Hutcheson of Scientific Materials Corporation of Bozeman, MT for providing the crystals. This research was supported by AFOSR Grant Number F49620-00-1-0314, Montana Board of Research and Commercialization Technology, and NSF Grant Number 0125429 – Partnerships for Innovation.

REFERENCES

1. W. R. Babbitt "Memory, processing, and routing applications of spatial-spectral holography in ultra-high speed computing systems", Proc. SPIE **3468**, pp. 304-311, 1998; A. Renn, U. P. Wild, and A. Rebane, "Multidimensional Holography by Persistent Spectral Holeburning", J. Phys. Chem. A **106**, pp. 3045-3060, 2002.

2. H. Lin, T. Wang, and T. W. Mossberg, "Demonstration of 8-Gbit/in.^{2} areal storage density based on swept-carrier frequency-selective optical memory", Opt. Lett. **20**, pp. 1658-1660, 1995.

3. P. B. Sellin, N. M. Strickland, T. Böttger, J. L. Carlsten, and R. L. Cone, "Laser Stabilization at 1536 nm Using Regenerative Spectral Hole Burning", Phys. Rev. B **63,** pp. 155111-1 - 155111-7, 2001; T. Böttger, G. J. Pryde, N. M. Strickland, P. B. Sellin, and R. L. Cone, "Semiconductor Lasers Stabilized to Spectral Holes in Rare-Earth Crystals", Optics & Photonics News **12**, no.12, p. 23, Dec. 2001; G. J. Pryde, T. Böttger, and R. L. Cone "Numerical Modeling of Laser Stabilization by Regenerative Spectral Holeburning", J. of Lumin 94, pp. 587-591, 2001; G. J. Pryde, T. Böttger, R. L. Cone, "Semiconductor Lasers Stabilized to Spectral Holes in Rare Earth Crystals to a Part in 10^{13} and their Application to Devices and Spectroscopy", J. of Lumin. **98**, pp. 309-315, 2002; T. Böttger, G. J. Pryde, and R. L. Cone, "Programmable laser frequency stabilization at 1523 nm by use of persistent spectral hole burning", to appear, Opt. Lett. **28**, 2003.

4. M. D. Lukin, P. R. Hemmer, "Quantum Entanglement via Optical Control of Atom-Atom Interactions", Phys. Rev. Lett. **84**, pp. 2818-2821, 2000; N. Ohlsson, R. K. Mohan, S. Kröll, "Quantum computer hardware based on rare-earth-ion-doped inorganic crystals", Opt. Comm. **201**, pp. 71-77, 2002; J. J. Longdell, M. J. Sellars, "Experimental demonstration of quantum state tomography applied to dopant ions in a solid", submitted to Phys. Rev. Lett. 2002.

5. K. D. Merkel, R. D. Peters, P. B. Sellin, K. S. Repasky, and W. R. Babbitt, "Accumulated programming of a complex spectral grating", Opt. Lett. **25**, pp. 1627-1629, 2000.

6. R. M. Macfarlane, T. L. Harris, Y. Sun, R. L. Cone, and R. W. Equall, "Measurement of photon echoes in Er:Y_2SiO_5 at 1.5 μm with a diode laser and an amplifier", Opt. Lett. **22**, pp. 871-873, 1997.

7. T. L. Harris, Y. Sun, R. L. Cone, R. M. Macfarlane, and R. W. Equall, "Demonstration of real-time address header decoding for optical data routing at 1536 nm", Opt. Lett. **23**, pp. 636-638, 1998.

8. T. L. Harris, Y. Sun, W. R. Babbitt, R. L. Cone, J. A. Ritcey, and R. W. Equall, "Spatial-spectral holographic correlator at 1536 nm using 30-symbol quadriphase- and binary-phase-shift keyed codes", Opt. Lett. **25**, pp. 85-87, 2000.

9. Z. Cole, T. Böttger, R. Krishna Mohan, R. Reibel, W. R. Babbitt, R. L. Cone and K. D. Merkel, "Coherent integration of 0.5 GHz spectral holograms at 1536 nm using dynamic bi-phase codes", Appl. Phys. Lett. **81**, pp. 3525-3527, 2002.

10. C. Li, C. Wyon, and Richard Moncorgé, " Spectroscopic Properties and Fluorescence Dynamics of Er^{3+} and Yb^{3+} in Y_2SiO_5", IEEE J. Quant. Elect. **28**, pp. 1209-1221, 1992.

11. B. A. Maksimov, Yu. A. Kharitonov, V. V. Ilyukhin and N. B. Belov, "Crystal Structure of the Y-Oxysilicate $Y_2(SiO_4)O$", Sov. Phys. Doklady **13**, pp. 1188-1189, 1969.

12. Obtained from the HITRAN database of the Harvard-Smithsonian Center for Astrophysics.

13. T. Böttger, "Laser frequency stabilization to spectral hole burning frequency references in Erbium-doped crystals: material and device optimization", PhD thesis, Montana State University, 2002.

14. T. Böttger, Y. Sun, C. W. Thiel, and R. L. Cone to be published.

15. Y. Sun, G. M. Wang, R. L. Cone, R. W. Equall, M. J. M. Leask, "Symmetry considerations regarding light propagation and light polarization for coherent interactions with ions in crystals", Phys. Rev. B **62**, pp. 15443-15451, 2000.

16. T. Böttger, Y. Sun, G.J. Pryde, G. Reinemer, and R.L. Cone, "Diode laser frequency stabilization to transient spectral holes and spectral diffusion in Er^{3+}:Y_2SiO_5 at 1536 nm", J. Lumin. **94-95**, pp. 565-568, 2001.

17. W. B. Mims, Phys. Rev. **168**, "Phase Memory in Electron Spin Echoes, Lattice Relaxation Effects in $CaWO_4$:Er, Ce, Mn", pp. 370-389, 1968; W. B. Mims "Electron Spin Echoes" in *Electron Paramagnetic Resonance*, edited by S. Geschwind, Plenum Press New York, pp. 263-351, 1972.

18. T. Böttger, C. W. Thiel, Y. Sun and R. L. Cone to be published.

19. G. K. Liu and R. L. Cone "Laser-induced instantaneous spectral diffusion in Tb^{3+} compounds as observed in photon-echo experiments", Phys. Rev. B **41**, pp. 6193-6200, 1990.

20. R. Orbach and H. J. Stapleton "Electron Spin-Lattice Relaxation", in *Electron Paramagnetic Resonance*, edited by S. Geschwind, Plenum Press New York, pp. 121-216, 1972.

21. D. J. Singel, private communication, 2002.

22. R. W. Equall, Y. Sun, R. L. Cone, and R. M. Macfarlane, "Ultra slow optical dephasing in Eu^{3+}:Y_2SiO_5", Phys. Rev. Lett. **72**, pp. 2179-2184, 1994.